

Discriminant indicators with generalized inversion symmetry

Tsuneya Yoshida¹, Ryo Okugawa², and Yasuhiro Hatsugai¹

¹ *Department of Physics, University of Tsukuba, Ibaraki 305-8571, Japan and*

² *Graduate School of Information Sciences, Tohoku University, Sendai 980-8579, Japan*

(Dated: November 16, 2021)

We propose indicators of the discriminant for systems with generalized inversion symmetry which are computed from data only at high-symmetry points in the Brillouin zone. Our approach captures the exceptional points and their symmetry-protected variants without ambiguity arising from the reference energy, which is advantage over the previously known indicators for non-Hermitian systems. As demonstrations, we systematically analyze 3×3 -Hamiltonians where the proper choice of the reference energy is not obvious.

I. INTRODUCTION

Non-Hermitian topology is studied as one of current hot topics attracting broad attention^{1–6}. When the Hermiticity is violated, systems exhibit novel topological phenomena due to the point-gap topology for which the non-Hermiticity is essential^{7–14}. A representative example is the non-Hermitian skin effect which results in extreme sensitivity of eigenstates and eigenvectors to the presence/absence of boundaries^{8,15–18}. Another typical example is the emergence of exceptional points^{19–23} on which energy bands touch for both of the real- and imaginary-parts. The topology of exceptional points is further enriched by symmetry^{24–27}; symmetry-protected exceptional rings (SPERs) and symmetry-protected exceptional surfaces (SPESs) emerge in two and three dimensions. Among studies of non-Hermitian systems, searching platforms of the above topological phenomena is considered to be an important issue in terms of applications and has been addressed extensively. So far, exceptional points and skin effects have been reported for open quantum systems^{28–32}, photonic systems^{33–41}, mechanical systems^{42–44}, electric circuits^{45–47}, quasi-particle spectrum^{48–55} and so on.

For further search of the platforms, indicators are considered to be powerful tools; in Hermitian case, symmetry-indicators are employed as efficient filters^{56–59} of trivial topology and allow systematic search of topological insulators and semimetals. Symmetry-indicators are also extended to non-Hermitian cases^{60–65}. In particular, Refs. 60–62 introduced indicators for exceptional points and the skin effects by analyzing the doubled Hermitian Hamiltonian which is composed of the non-Hermitian Hamiltonian and the reference energy. However, these previously introduced indicators possess ambiguity arising from the reference energy, which prevent us from systematically searching the non-Hermitian topological phenomena.

In this paper, we propose another type of the indicators by focusing on the discriminant which allows to characterize exceptional points without input of the reference energy^{66–68}. Our discriminant indicators allow systematic search of exceptional points and symmetry-protected variants (i.e., SPERs and SPESs) for systems

with generalized inversion symmetry. The above advantage is demonstrated by analyzing non-Hermitian Hamiltonians where a proper choice of the reference energy is not obvious.

The rest of this paper is organized as follows. After a brief review of the discriminant in Sec. II, we introduce the discriminant indicator for systems with generalized inversion symmetry in Sec. III where a numerical simulation is also performed. In Sec. IV, we propose the discriminant indicator for SPERs and SPESs for generalized time-reversal and inversion symmetric systems. A short summary is given in Sec. V. Appendices are devoted to details of the discriminant (Appendix A), relations between symmetry indicators and discriminant indicators (Appendix B), and details of symmetry constraints (Appendix C).

II. BRIEF REVIEW OF THE DISCRIMINANT AND EXCEPTIONAL POINTS

Consider a two-dimensional system which is described by a 2×2 -Hamiltonian $H(\mathbf{k})$. Exceptional points in this system is characterized by the following winding number²³

$$\nu_{2 \times 2} = \oint \frac{d\mathbf{k}}{2\pi i} \cdot \nabla_{\mathbf{k}} \log[\epsilon_1(\mathbf{k}) - \epsilon_2(\mathbf{k})], \quad (1)$$

where $\epsilon_n(\mathbf{k})$ ($n = 1, 2$) denote eigenvalues of the Hamiltonian. The integral is taken along a closed path. The operator $\nabla_{\mathbf{k}}$ is defined as $\nabla_{\mathbf{k}} := (\partial_{k_x}, \partial_{k_y})$. Here, ∂_{k_x} (∂_{k_y}) denotes derivative respect to k_x (k_y) where k_x and k_y are x - and y - components of the momentum respectively.

The discriminant number is introduced as an generalized version of $\nu_{2 \times 2}$ to an $N \times N$ -Hamiltonian $H(\mathbf{k})$ ^{66–68}.

$$\nu = \oint \frac{d\mathbf{k}}{2\pi i} \cdot \nabla_{\mathbf{k}} \log \Delta(\mathbf{k}). \quad (2)$$

Here, $\Delta(\mathbf{k})$ denotes the discriminant of the polynomial $\det[H(\mathbf{k}) - E\mathbf{1}] = a_N(-E)^N + a_{N-1}(-E)^{N-1} + \dots + a_0$ ($a_l \in \mathbb{C}$) which is defined as

$$\Delta(\mathbf{k}) := (-1)^{N(N-1)/2} \prod_{n \neq n'} (\epsilon_n - \epsilon_{n'}), \quad (3)$$

with ϵ_n being roots of the polynomial [i.e., eigenvalues of $H(\mathbf{k})$]. We note that the discriminant is written in terms of a_i 's (for more details see Appendix A). If the discriminant number takes a non-trivial value for a closed path in the Brillouin zone (BZ), $\Delta(\mathbf{k})$ vanishes at a point inside of the loop. Therefore, at least two bands touch at this point [see Eq. (3)].

Another generalization is the following winding number⁶⁹

$$W(E_{\text{ref}}) = \oint \frac{d\mathbf{k}}{2\pi i} \cdot \nabla_{\mathbf{k}} \log \det[H(\mathbf{k}) - E_{\text{ref}}\mathbb{1}], \quad (4)$$

where E_{ref} is chosen as the energy at which an exceptional point emerge. In other words, for the characterization by $W(E_{\text{ref}})$, one needs to know a proper choice of E_{ref} by diagonalizing the Hamiltonian. The advantage of the discriminant number is that one does not need to know energy at which two bands touch apriori.

III. INDICATORS FOR GENERALIZED INVERSION SYMMETRIC SYSTEMS

Consider a system with generalized inversion symmetry which is written as

$$U_I H(\mathbf{k}) U_I^\dagger = H^\dagger(-\mathbf{k}), \quad (5)$$

where U_I is a Hermitian and unitary matrix (i.e., $U_I U_I^\dagger = \mathbb{1}$ and $U_I^\dagger = U_I$).

Equation (5) results in the following constraint on the discriminant:

$$\Delta(\mathbf{k}) = \Delta^*(-\mathbf{k}), \quad (6)$$

which is proven in Sec. III A [see Eq. (9)-Eq. (11)].

As we see below, the symmetry constraint on the discriminant allows to define the indicator (7) [Eq. (16)] which captures exceptional points [exceptional loops] in two dimensions [three dimensions].

A. Two dimensions

Consider the discriminant number ν computed along the closed path illustrated in Fig. 1(a). The generalized inversion symmetry imposes the following constraint on the parity of ν

$$(-1)^\nu = \zeta_{\text{I,2D}} := \prod_{\mathbf{\Gamma}_j \in \text{TRIM}} \text{sgn} \Delta(\mathbf{\Gamma}_j), \quad (7)$$

where TRIM denotes time-reversal symmetric momenta

$$\text{TRIM} = \{(0, 0), (\pi, 0), (0, \pi), (\pi, \pi)\}. \quad (8)$$

We note that $\Delta(\mathbf{\Gamma}_j)$ ($\mathbf{\Gamma}_j \in \text{TRIM}$) are real because of Eq. (6). Equation (7) means that $\zeta_{\text{I,2D}}$ taking -1 indicates the emergence of exceptional points.

Eigenvalues of the inversion operator do not explicitly appear in Eq. (7), while the indicator computed from the

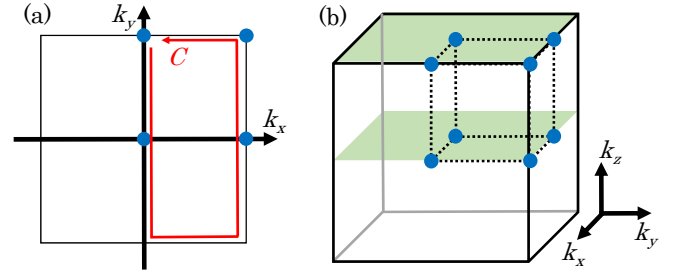


FIG. 1. (a) [(b)]: Sketch of the BZ of the square [cubic] lattice, $-\pi < k_\mu \leq \pi$ with $\mu = x, y$ [$\mu = x, y, z$]. Blue dots denotes TRIM which are invariant under the transformation $\mathbf{k} \rightarrow -\mathbf{k}$. Red lines in panel (a) denotes a closed path where the integral in Eq. (2) is computed.

eigenvalues of symmetry operators in Hermitian case. We note, however, that the product of parity eigenvalues is computed in right hand side of Eq. (7), which is discussed in Appendix B.

Equation (7) can be proven by taking into account the symmetry constraint [Eq. (5)]. As a first step, we prove Eq. (6). Let $|R_n(\mathbf{k})\rangle$ and $|L_n(\mathbf{k})\rangle$ be right and left eigenvectors of $H(\mathbf{k})$

$$H(\mathbf{k})|R_n(\mathbf{k})\rangle = \epsilon_n(\mathbf{k})|R_n(\mathbf{k})\rangle, \quad (9a)$$

$$H^\dagger(\mathbf{k})|L_n(\mathbf{k})\rangle = \epsilon_n^*(\mathbf{k})|L_n(\mathbf{k})\rangle. \quad (9b)$$

Then, we have

$$\begin{aligned} H(-\mathbf{k})U_I|L_n(\mathbf{k})\rangle &= U_I H^\dagger(\mathbf{k})|L_n(\mathbf{k})\rangle \\ &= \epsilon_n^*(\mathbf{k})U_I|L_n(\mathbf{k})\rangle, \end{aligned} \quad (10)$$

which results in

$$\epsilon_n^*(-\mathbf{k}) = \epsilon_n(\mathbf{k}). \quad (11)$$

Combining Eq. (3) and Eq. (11), we obtain Eq. (6).

Now, we evaluate the discriminant number along the path illustrated in Fig. 1(a). Firstly, we decompose the integral into two parts

$$\nu = \nu_0 - \nu_\pi, \quad (12)$$

with

$$2\pi i \nu_{k_0} = \int_{-\pi}^{\pi} dk_y \partial_{k_y} \log \Delta(k_0, k_y), \quad (13)$$

$\Delta(k_x, k_y) := \Delta(\mathbf{k})$, and k_0 taking 0 or π . Because the inversion is closed for one-dimensional subsystems specified

by $k_0 = 0, \pi$, the integral can be simplified as follows^{70,71}:

$$\begin{aligned}
& 2i\pi\nu_{k_0} \\
&= \int_0^\pi dk_y \partial_{k_y} \log \Delta(k_0, k_y) + \int_{-\pi}^0 dk_y \partial_{k_y} \log \Delta(k_0, k_y) \\
&= \int_0^\pi dk_y \partial_{k_y} \log \Delta(k_0, k_y) + \int_{-\pi}^0 dk_y \partial_{k_y} \log \Delta^*(k_0, -k_y) \\
&= \int_0^\pi dk_y \partial_{k_y} \log \Delta(k_0, k_y) - \int_0^\pi dp_y \partial_{p_y} \log \Delta^*(k_0, p_y) \\
&= 2i\text{Im} \int_0^\pi dk_y \partial_{k_y} \log \Delta(k_0, k_y) \\
&= 2i [\text{Arg}\Delta(k_0, \pi) - \text{Arg}\Delta(k_0, 0) + 2\pi N_0], \tag{14}
\end{aligned}$$

with an integer N_0 . Here, from the second to the third line, we have used Eq. (6). Taking a principal value $[-\pi < \text{Arg}\Delta(\mathbf{k}) \leq \pi]$ results in N_0 ambiguity in the last line. The above results indicate the following relation

$$\begin{aligned}
e^{i\pi\nu_{k_0}} &= e^{i[\text{Arg}\Delta(k_0, \pi) - \text{Arg}\Delta(k_0, 0)]} \\
&= \text{sgn}\Delta(k_0, \pi)\text{sgn}\Delta(k_0, 0). \tag{15}
\end{aligned}$$

Putting Eqs. (12) and (15) together, we end up with Eq. (7).

In the above, we have assumed that $\Delta(\mathbf{k})$ is non-zero along the path denoted by red lines in Fig. 1(a). We note, however, that zeros of $\Delta(\mathbf{k})$ on the path but away from TRIM does not change the conclusion. This is because we can take another path where the inversion is closed and $\Delta(\mathbf{k})$ is finite⁷².

B. Three dimensions

Generically, exceptional points form a loop in the three-dimensional BZ $[-\pi < k_\mu \leq \pi$ ($\mu = x, y, z$)]³¹. In this case, focusing on $k_z = 0, \pi$, the problem is reduced to the case discussed in Sec. III A [see green planes in Fig. 1(b)]. Thus, we can use the following indicator to detect the exceptional loop

$$\zeta_{\text{I,3D}} := \prod_{\Gamma_j \in \text{TRIM}} \text{sgn}\Delta(\Gamma_j), \tag{16}$$

where TRIM denotes time-reversal symmetric momenta⁷³

$$\begin{aligned}
\text{TRIM} = \{ & (0, 0, 0), (\pi, 0, 0), (0, \pi, 0), (\pi, \pi, 0), \\
& (0, 0, \pi), (\pi, 0, \pi), (0, \pi, \pi), (\pi, \pi, \pi) \}. \tag{17}
\end{aligned}$$

C. Application to a toy model

Now, we apply the above approach to a toy model in two dimensions where a proper value of the reference

energy is not obvious. The Hamiltonian reads

$$\begin{aligned}
H(\mathbf{k}) = & \xi(\mathbf{k}) \begin{pmatrix} \frac{1}{2} & 0 & 0 \\ 0 & 0 & 1 \\ 0 & 1 & 0 \end{pmatrix} + (i\gamma + \sin k_x) \begin{pmatrix} 0 & 0 & 0 \\ 0 & 0 & -i \\ 0 & i & 0 \end{pmatrix} \\
& + (i\gamma + \sin k_y) \begin{pmatrix} 0 & 0 & 0 \\ 0 & 1 & 0 \\ 0 & 0 & -1 \end{pmatrix} + \xi'(\mathbf{k}) \begin{pmatrix} 0 & \frac{1}{2} & -\frac{1}{2} \\ \frac{1}{2} & 0 & i \\ -\frac{1}{2} & i & 0 \end{pmatrix} \\
& + \xi''(\mathbf{k}) \begin{pmatrix} 1 & 0 & 0 \\ 0 & 0 & 0 \\ 0 & 0 & 0 \end{pmatrix}, \tag{18}
\end{aligned}$$

with $\xi(\mathbf{k}) = -2t(\cos k_x + \cos k_y) - m$, $\xi'(\mathbf{k}) = 0.3i \cos(k_x + k_y) + 0.5 \sin(k_x - k_y)$, and $\xi''(\mathbf{k}) = 0.3i \sin(k_x - k_y) + 2 \cos(k_x + k_y)$. Parameters m , t , and γ are real numbers. This Hamiltonian preserves the generalized inversion symmetry [see Eq. (5)] with

$$U_I = \begin{pmatrix} 1 & 0 & 0 \\ 0 & 0 & 1 \\ 0 & 1 & 0 \end{pmatrix}. \tag{19}$$

We note that the above Hamiltonian with generalized inversion symmetry can be obtained by

$$H(\mathbf{k}) = \frac{1}{2} [H_0(\mathbf{k}) + U_I H_0^\dagger(-\mathbf{k}) U_I^\dagger], \tag{20}$$

with a general Hamiltonian $H_0(\mathbf{k})$.

Figure 2(a) plots a phase diagram against m and γ for $t = 0.5$. It indicates that exceptional points emerge in the region colored with pink. For the sake of concreteness, let us focus on the case of $(m, t, \gamma) = (-3, 0.5, 2)$ [see the black dot in Fig. 2(a)]. Figure 2(b) is a color plot of $\text{Arg}\Delta(\mathbf{k})/\pi$ in the momentum space for $(m, t, \gamma) = (-3, 0.5, 2)$. It indicates that the discriminant number computed along the path illustrated in Fig. 1(a) takes -3 , which is consistent with the discriminant indicator taking -1 . Exceptional points emerge at points denoted by orange and green dots in Fig. 2(b), which can be confirmed in Figs. 2(c) and 2(d). The above results indicate that the discriminant indicator successfully captures the exceptional points.

We finish this part with a remark on the indicator in previous works^{60–62},

$$(-1)^{W(E_{\text{ref}})} = \prod_{\Gamma_j \in \text{TRIM}} \text{sgn}(\det[H(\Gamma_j) - E_{\text{ref}}\mathbb{1}]). \tag{21}$$

To compute this indicator, one needs to know a proper choice of E_{ref} by analyzing the band structure. In addition, changing a parameter (e.g., m or γ) shifts the energy where two bands touch. These behaviors prevent us from systematically searching the exceptional points based on Eq. (21). In contrast, one can carry out a systematic analysis by discriminant indicators [Eqs. (7) and (16)].

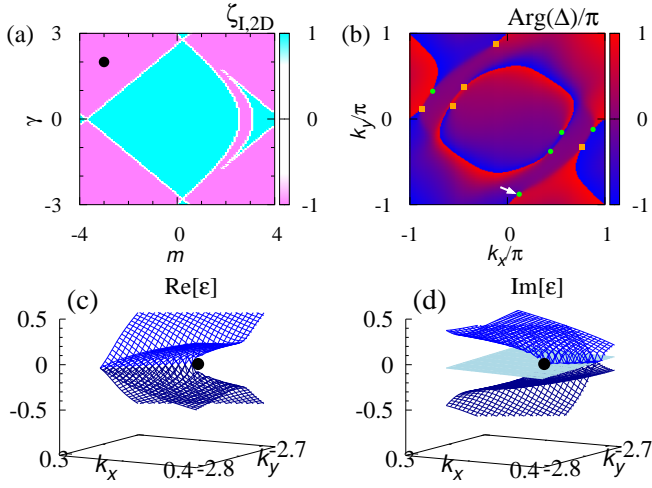


FIG. 2. (a): Discriminant indicator $[\zeta_{I,2D} = (-1)^\nu]$ for $t = 0.5$. (b): Argument of $\Delta(\mathbf{k})$ normalized by π in the BZ. The orange (green) symbols denote exceptional points with $\nu = 1$ (-1). (c) [(d)]: The real- (imaginary-) part of the energy bands around \mathbf{k}_{EP1} . These data are obtained for $(m, t, \gamma) = (-3, 0.5, 2)$ [see the black dot in panel (a)].

IV. INDICATORS FOR GENERALIZED TIME-REVERSAL AND INVERSION SYMMETRIC SYSTEMS

A. Two and three dimensions

Consider generalized time-reversal and inversion symmetric systems

$$U_T H^T(\mathbf{k}) U_T^\dagger = H(-\mathbf{k}), \quad (22a)$$

$$U_I H^\dagger(\mathbf{k}) U_I^\dagger = H(-\mathbf{k}), \quad (22b)$$

with unitary operators U_T and U_I satisfying $U_T U_T^* = \mathbb{1}$ and $U_I U_I = \mathbb{1}$, respectively. In Ref. 13, symmetry described by Eq. (22a) is denoted as TRS^\dagger . In two (three) dimensions, the systems host SPERs (SPESs) which are characterized by the sign of the discriminant^{68,74}.

In order to introduce an indicator for these symmetry-protected topological properties, let us start with the following constraints imposed by symmetry Eq. (22):

$$\Delta(\mathbf{k}) = \Delta^*(\mathbf{k}), \quad (23a)$$

$$\Delta(\mathbf{k}) = \Delta(-\mathbf{k}), \quad (23b)$$

which are proven in Sec. IV B. Because the real function $\Delta(\mathbf{k})$ is continuous and inversion symmetric, we can introduce the following indicator for SPERs and SPESs,

$$\zeta_{\text{TI}} = \prod_{\Gamma_j \in \text{TRIM}} \text{sgn} \Delta(\Gamma_j). \quad (24)$$

When ζ_{TI} takes -1 , SPERs (SPESs) emerge in the two-(three-) dimensional BZ.

The above indicator also works for systems with another type of time-reversal and inversion symmetry

$$U_T H^*(\mathbf{k}) U_T^\dagger = H(-\mathbf{k}), \quad (25a)$$

$$U_I H(\mathbf{k}) U_I^\dagger = H(-\mathbf{k}), \quad (25b)$$

with $U_T U_T^* = \mathbb{1}$ because the above constraint results in Eq. (23) (see Appendix C).

B. Proof of Eq. (23)

When the Hamiltonian satisfies Eq. (22), we obtain Eq. (23). Firstly, we note that energy eigenvalues satisfy

$$\epsilon_n(-\mathbf{k}) = \epsilon_n(\mathbf{k}), \quad (26)$$

in the presence of the generalized time-reversal symmetry, which is proven as follows. Let $|L_n(\mathbf{k})\rangle$ be left eigenvectors of $H(\mathbf{k})$ with eigenvalues $\epsilon_n(\mathbf{k})$ ($n = 1, 2, 3, \dots$) [see Eq. (9b)]. Then, we have $U_T \mathcal{K} |L_n(\mathbf{k})\rangle$ as right eigenvectors of $H(-\mathbf{k})$ with eigenvalues $\epsilon_n(\mathbf{k})$

$$\begin{aligned} H(-\mathbf{k}) U_T \mathcal{K} |L_n(\mathbf{k})\rangle &= U_T H^T(\mathbf{k}) \mathcal{K} |L_n(\mathbf{k})\rangle \\ &= U_T \mathcal{K} H^\dagger(\mathbf{k}) |L_n(\mathbf{k})\rangle \\ &= \epsilon_n(\mathbf{k}) U_T \mathcal{K} |L_n(\mathbf{k})\rangle, \end{aligned} \quad (27)$$

where \mathcal{K} is a complex conjugation operator. This relation prove that Eq. (26) holds. Equation (26) results in Eq. (23b), which can be seen by noting that $\Delta(\mathbf{k})$ is computed from the energy eigenvalues $\epsilon_n(\mathbf{k})$ [see Eq. (3)]. As we have seen in Sec. III A, the generalized inversion symmetry results in $\Delta(\mathbf{k}) = \Delta^*(-\mathbf{k})$ [see Eq. (6)]. Thus, combining this equation and Eq. (23b), we obtain Eq. (23a).

C. Application to a toy model

We demonstrate that the indicator [Eq. (24)] captures the SPERs in two dimensions even when energy where two band touch depends on momentum. Let us analyze the following 3×3 -Hamiltonian $H(\mathbf{k})$ in two dimensions

$$\begin{aligned} H(\mathbf{k}) &= i\xi(\mathbf{k}) \begin{pmatrix} 0 & 0 & 0 \\ 0 & 1 & 0 \\ 0 & 0 & -1 \end{pmatrix} + it \sin k_x \begin{pmatrix} 0 & 0 & 0 \\ 0 & 0 & 1 \\ 0 & -1 & 0 \end{pmatrix} \\ &+ t \sin k_y \begin{pmatrix} 0 & 1 & 1 \\ -1 & 0 & 0 \\ -1 & 0 & 0 \end{pmatrix} + \gamma \cos k_x \begin{pmatrix} 1 & 0 & 0 \\ 0 & 0 & 0 \\ 0 & 0 & 0 \end{pmatrix} \\ &+ \gamma \cos(k_x + k_y) \begin{pmatrix} 0 & 1 & 1 \\ 1 & 0 & 0 \\ 1 & 0 & 0 \end{pmatrix}, \end{aligned} \quad (28)$$

with $\xi(\mathbf{k}) = \cos k_x + \cos k_y - m$. This Hamiltonian satisfies Eqs. (22a) and (22b) with $U_T = \mathbb{1}$ and U_I defined in Eq. (19).

The phase diagram is shown in Fig. 3(a). In the region colored with pink, the indicator takes -1 and predicts the

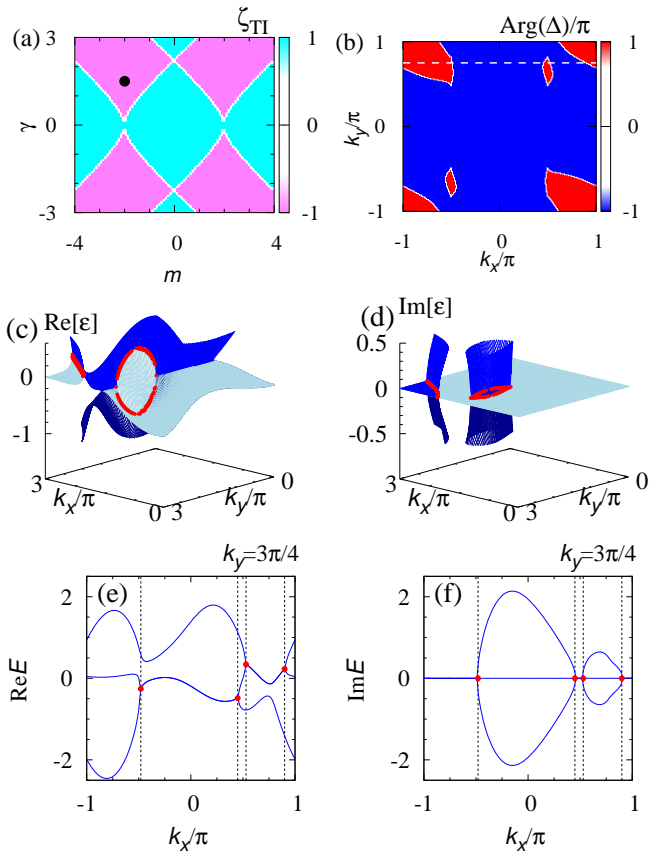


FIG. 3. (a): The indicator for $t = 0.5$. The black dot denotes a parameter set $(m, \gamma) = (-2, 1.5)$. (b): Sign of the discriminant $\Delta(\mathbf{k})$ in the BZ. (c) [(d)]: The real- (imaginary-) part of the energy bands for $0 \leq k_x \leq \pi$ and $0 \leq k_y \leq \pi$. (e) [(f)]: The real- (imaginary-) part of the energy bands for $-\pi \leq k_x \leq \pi$ and $k_y = 3\pi/4$ [see also dashed line in panel (b)]. Panels (b)-(f) are obtained for $(m, t, \gamma) = (-2, 0.5, 1.5)$.

emergence of SPERs. Figure 3(b) displays $\text{sgn}\Delta(\mathbf{k})$ for $(m, t, \gamma) = (-2, 0.5, 1.5)$ [see the black dot in Fig. 3(a)]. In this figure, we can see regions where $\text{sgn}\Delta(\mathbf{k})$ takes 1 or -1. On the boundaries, the discriminant $\Delta(\mathbf{k})$ becomes zero. Correspondingly, the two bands touch as shown in Fig. 3(c) and 3(d), which indicates the emergence of SPERs.

We finish this part with a remark on an indicator

$$z_{\text{TI}} = \prod_{\Gamma_j \in \text{TRIM}} \text{sgn}(\det[H(\Gamma_j) - E_{\text{ref}}\mathbb{1}]), \quad (29)$$

with $E_{\text{ref}} \in \mathbb{R}$. Detecting the above SPERs with this indicator is difficult because the energy where two bands touch depends on the momentum [see Figs. 3(e) and 3(f)]. Figure 3 indicates that the indicator defined in Eq. (24) captures SPERs even in this case.

V. SUMMARY

In this paper, we have proposed the discriminant indicator for systems with generalized inversion symmetry. In contrast to the previously introduced indicators, our approach captures exceptional points without ambiguity arising from the choice of the reference energy. A similar indicator is also introduced for SPERs (SPERs) in two- (three-) dimensional systems with generalized inversion and time-reversal symmetry. Applying the discriminant indicators to 3×3 -Hamiltonians, we have demonstrated that our approach successfully captures exceptional points and SPERs even when a proper choice of the reference energy is not obvious.

We finish this paper with two remarks. Firstly, we note that the previously introduced indicators^{60–62} are also applicable to skin effects, while our indicators focus only on exceptional points and their symmetry-protected variants. Secondly, we note that while indicators for the line-gap topology has been discussed for correlated systems^{64,65}, indicators for the point-gap topology have not been discussed so far. Introducing indicators for correlated systems is expected to accelerate search of the non-Hermitian topology of such systems which is left as a future work to be addressed.

ACKNOWLEDGMENTS

T. Y. and Y. H. thank Pierre Delplace for discussion on the discriminant in the previous work⁶⁸. This work is supported by JSPS Grant-in-Aid for Scientific Research on Innovative Areas “Discrete Geometric Analysis for Materials Design”: Grants No. JP17H06469 and No. JP20H04627. This work is also supported by JSPS KAKENHI Grants No. JP17H06138, No. JP20K14371, and No. JP21K13850.

¹ N. Hatano and D. R. Nelson, Phys. Rev. Lett. **77**, 570 (1996).

² C. M. Bender and S. Boettcher, Phys. Rev. Lett. **80**, 5243 (1998).

³ Y. C. Hu and T. L. Hughes, Phys. Rev. B **84**, 153101 (2011).

⁴ K. Esaki, M. Sato, K. Hasebe, and M. Kohmoto, Phys. Rev. B **84**, 205128 (2011).

⁵ E. J. Bergholtz, J. C. Budich, and F. K. Kunst, Rev. Mod. Phys. **93**, 015005 (2021).

⁶ Y. Ashida, Z. Gong, and M. Ueda, Advances in Physics **69**, 249 (2020).

⁷ V. M. Martinez Alvarez, J. E. Barrios Vargas, and L. E. F. Foa Torres, Phys. Rev. B **97**, 121401 (2018).

⁸ S. Yao and Z. Wang, Phys. Rev. Lett. **121**, 086803 (2018).

- ⁹ S. Yao, F. Song, and Z. Wang, Phys. Rev. Lett. **121**, 136802 (2018).
- ¹⁰ F. K. Kunst, E. Edvardsson, J. C. Budich, and E. J. Bergholtz, Phys. Rev. Lett. **121**, 026808 (2018).
- ¹¹ K. Yokomizo and S. Murakami, Phys. Rev. Lett. **123**, 066404 (2019).
- ¹² Z. Gong, Y. Ashida, K. Kawabata, K. Takasan, S. Higashikawa, and M. Ueda, Phys. Rev. X **8**, 031079 (2018).
- ¹³ K. Kawabata, K. Shiozaki, M. Ueda, and M. Sato, Phys. Rev. X **9**, 041015 (2019).
- ¹⁴ H. Zhou and J. Y. Lee, Phys. Rev. B **99**, 235112 (2019).
- ¹⁵ C. H. Lee and R. Thomale, Phys. Rev. B **99**, 201103 (2019).
- ¹⁶ D. S. Borgnia, A. J. Kruchkov, and R.-J. Slager, Phys. Rev. Lett. **124**, 056802 (2020).
- ¹⁷ K. Zhang, Z. Yang, and C. Fang, Phys. Rev. Lett. **125**, 126402 (2020).
- ¹⁸ N. Okuma, K. Kawabata, K. Shiozaki, and M. Sato, Phys. Rev. Lett. **124**, 086801 (2020).
- ¹⁹ T. Katō, *Perturbation theory for linear operators*, Vol. 132 (Springer, 1966).
- ²⁰ I. Rotter, Journal of Physics A: Mathematical and Theoretical **42**, 153001 (2009).
- ²¹ M. V. Berry, Czechoslovak Journal of Physics **54**, 1039 (2004).
- ²² W. D. Heiss, J. Phys. A **45**, 444016 (2012).
- ²³ H. Shen, B. Zhen, and L. Fu, Phys. Rev. Lett. **120**, 146402 (2018).
- ²⁴ J. C. Budich, J. Carlström, F. K. Kunst, and E. J. Bergholtz, Phys. Rev. B **99**, 041406 (2019).
- ²⁵ R. Okugawa and T. Yokoyama, Phys. Rev. B **99**, 041202 (2019).
- ²⁶ T. Yoshida, R. Peters, N. Kawakami, and Y. Hatsugai, Phys. Rev. B **99**, 121101 (2019).
- ²⁷ H. Zhou, J. Y. Lee, S. Liu, and B. Zhen, Optica **6**, 190 (2019).
- ²⁸ L. Jin and Z. Song, Phys. Rev. A **80**, 052107 (2009).
- ²⁹ P. San-Jose, J. Cayao, E. Prada, and R. Aguado, Scientific Reports **6**, 21427 (2016).
- ³⁰ T. E. Lee, Phys. Rev. Lett. **116**, 133903 (2016).
- ³¹ Y. Xu, S.-T. Wang, and L.-M. Duan, Phys. Rev. Lett. **118**, 045701 (2017).
- ³² L. Jin and Z. Song, Phys. Rev. A **80**, 052107 (2009).
- ³³ A. Guo, G. J. Salamo, D. Duchesne, R. Morandotti, M. Volatier-Ravat, V. Aimez, G. A. Siviloglou, and D. N. Christodoulides, Phys. Rev. Lett. **103**, 093902 (2009).
- ³⁴ C. E. Rüter, K. G. Makris, R. El-Ganainy, D. N. Christodoulides, M. Segev, and D. Kip, Nature physics **6**, 192 (2010).
- ³⁵ A. Regensburger, C. Bersch, M.-A. Miri, G. Onishchukov, D. N. Christodoulides, and U. Peschel, Nature **488**, 167 (2012).
- ³⁶ B. Zhen, C. W. Hsu, Y. Igarashi, L. Lu, I. Kaminer, A. Pick, S.-L. Chua, J. D. Joannopoulos, and M. Soljačić, Nature **525**, 354 (2015).
- ³⁷ A. U. Hassan, B. Zhen, M. Soljačić, M. Khajavikhan, and D. N. Christodoulides, Phys. Rev. Lett. **118**, 093002 (2017).
- ³⁸ K. Takata and M. Notomi, Phys. Rev. Lett. **121**, 213902 (2018).
- ³⁹ H. Zhou, C. Peng, Y. Yoon, C. W. Hsu, K. A. Nelson, L. Fu, J. D. Joannopoulos, M. Soljačić, and B. Zhen, **359**, 1009 (2018).
- ⁴⁰ T. Ozawa, H. M. Price, A. Amo, N. Goldman, M. Hafezi, L. Lu, M. C. Rechtsman, D. Schuster, J. Simon, O. Zilberberg, and I. Carusotto, Rev. Mod. Phys. **91**, 015006 (2019).
- ⁴¹ L. Xiao, T. Deng, K. Wang, G. Zhu, Z. Wang, W. Yi, and P. Xue, Nature Physics **16**, 761 (2020).
- ⁴² T. Yoshida and Y. Hatsugai, Phys. Rev. B **100**, 054109 (2019).
- ⁴³ A. Ghatak, M. Brandenbourger, J. van Wezel, and C. Coulais, Proceedings of the National Academy of Sciences **117**, 29561 (2020).
- ⁴⁴ C. Scheibner, W. T. M. Irvine, and V. Vitelli, Phys. Rev. Lett. **125**, 118001 (2020).
- ⁴⁵ T. Hofmann, T. Helbig, F. Schindler, N. Salgo, M. Brzezińska, M. Greiter, T. Kiessling, D. Wolf, A. Vollhardt, A. Kabaši, C. H. Lee, A. Bilušić, R. Thomale, and T. Neupert, Phys. Rev. Research **2**, 023265 (2020).
- ⁴⁶ T. Helbig, T. Hofmann, S. Imhof, M. Abdelghany, T. Kiessling, L. W. Molenkamp, C. H. Lee, A. Szameit, M. Greiter, and R. Thomale, Nature Physics **16**, 747 (2020).
- ⁴⁷ T. Yoshida, T. Mizoguchi, and Y. Hatsugai, Phys. Rev. Research **2**, 022062 (2020).
- ⁴⁸ V. Kozii and L. Fu, arXiv preprint arXiv:1708.05841 (2017).
- ⁴⁹ A. A. Zyuzin and A. Y. Zyuzin, Phys. Rev. B **97**, 041203 (2018).
- ⁵⁰ T. Yoshida, R. Peters, and N. Kawakami, Phys. Rev. B **98**, 035141 (2018).
- ⁵¹ H. Shen and L. Fu, Phys. Rev. Lett. **121**, 026403 (2018).
- ⁵² M. Papaj, H. Isobe, and L. Fu, Phys. Rev. B **99**, 201107 (2019).
- ⁵³ T. Matsushita, Y. Nagai, and S. Fujimoto, Phys. Rev. B **100**, 245205 (2019).
- ⁵⁴ Y. Michishita and R. Peters, Phys. Rev. Lett. **124**, 196401 (2020).
- ⁵⁵ T. Yoshida, R. Peters, N. Kawakami, and Y. Hatsugai, Progress of Theoretical and Experimental Physics **2020**, 12A109 (2020).
- ⁵⁶ C. Herring, Phys. Rev. **52**, 361 (1937).
- ⁵⁷ H. C. Po, A. Vishwanath, and H. Watanabe, Nature Communications **8**, 50 (2017).
- ⁵⁸ S. Ono and H. Watanabe, Phys. Rev. B **98**, 115150 (2018).
- ⁵⁹ H. C. Po, **32**, 263001 (2020).
- ⁶⁰ R. Okugawa, R. Takahashi, and K. Yokomizo, Phys. Rev. B **103**, 205205 (2021).
- ⁶¹ P. M. Vecsei, M. M. Denner, T. Neupert, and F. Schindler, Phys. Rev. B **103**, L201114 (2021).
- ⁶² K. Shiozaki and S. Ono, Phys. Rev. B **104**, 035424 (2021).
- ⁶³ R. Okugawa, R. Takahashi, and K. Yokomizo, Phys. Rev. B **102**, 241202 (2020).
- ⁶⁴ T. Yoshida, K. Kudo, H. Katsura, and Y. Hatsugai, Phys. Rev. Research **2**, 033428 (2020).
- ⁶⁵ S. Tsubota, H. Yang, Y. Akagi, and H. Katsura, arXiv preprint arXiv:2108.12860 (2021).
- ⁶⁶ C. C. Wojcik, X.-Q. Sun, T. c. v. Bzdušek, and S. Fan, Phys. Rev. B **101**, 205417 (2020).
- ⁶⁷ Z. Yang, A. P. Schnyder, J. Hu, and C.-K. Chiu, Phys. Rev. Lett. **126**, 086401 (2021).
- ⁶⁸ P. Delplace, T. Yoshida, and Y. Hatsugai, Phys. Rev. Lett. **127**, 186602 (2021).
- ⁶⁹ K. Kawabata, T. Bessho, and M. Sato, Phys. Rev. Lett. **123**, 066405 (2019).
- ⁷⁰ T. L. Hughes, E. Prodan, and B. A. Bernevig, Phys. Rev. B **83**, 245132 (2011).

- ⁷¹ Y. Hatsugai and I. Maruyama, Europhys. Lett. **95**, 20003 (2011).
⁷² Y. Kim, B. J. Wieder, C. L. Kane, and A. M. Rappe, Phys. Rev. Lett. **115**, 036806 (2015).
⁷³ Suppose that an exceptional loop extends from $k_z = -\pi$ to π . In such a case, computing $\zeta_{1,2D}$ for $k_z = 0, \pi$ captures this loop while $\zeta_{1,3D}$ takes 1.
⁷⁴ T. Yoshida, T. Mizoguchi, and Y. Hatsugai, arXiv preprint arXiv:2109.11127 (2021).

Appendix A: Details of the discriminant

Consider a polynomial

$$f(x) = a_N x^N + a_{N-1} x^{N-1} + \dots + a_1 x + a_0, \quad (\text{A1})$$

with $a_l \in \mathbb{C}$. The discriminant of $f(x)$ ($\text{Disc}[f(x)]$) is proportional to the resultant of $f(x)$ and $f'(x) := \partial_x f(x)$

$$(-1)^{N(N-1)/2} a_N \text{Disc}[f(x)] = \text{Res}[f(x), f'(x)]. \quad (\text{A2})$$

Here, ∂_x denotes derivative respect to x . Because the resultant $\text{Res}[f(x), f'(x)]$ is defined as the determinant of the Sylvester matrix,

$$\begin{aligned} & \text{Res}[f(x), f'(x)] \\ &= \det \begin{pmatrix} a_0 & 0 & \cdots & 0 & b_1 & 0 & \cdots & 0 \\ a_1 & a_0 & \ddots & \vdots & b_2 & b_1 & \ddots & \vdots \\ a_2 & a_1 & \ddots & a_0 & b_3 & b_2 & \ddots & 0 \\ \vdots & \vdots & \ddots & a_1 & \vdots & \vdots & \ddots & 0 \\ a_N & a_{N-1} & \cdots & a_2 & b_N & b_{N-1} & \cdots & b_1 \\ 0 & a_N & \ddots & \vdots & 0 & b_N & \ddots & b_2 \\ \vdots & \vdots & \ddots & a_{N-1} & \vdots & \vdots & \ddots & \vdots \\ 0 & 0 & \cdots & a_N & 0 & 0 & \cdots & b_N \end{pmatrix}, \end{aligned} \quad (\text{A3})$$

with $b_l = l a_l$, the discriminant can be written in terms of a_l ($l = 0, \dots, N$).

Specifically, for $N = 3$, we have

$$\begin{aligned} & \text{Res}[f(x), f'(x)] \\ &= \det \begin{pmatrix} a_0 & 0 & b_1 & 0 & 0 \\ a_1 & a_0 & b_2 & b_1 & 0 \\ a_2 & a_1 & b_3 & b_2 & b_1 \\ a_3 & a_2 & 0 & b_3 & b_2 \\ 0 & a_3 & 0 & 0 & b_3 \end{pmatrix}. \end{aligned} \quad (\text{A4})$$

Thus, the discriminant is written as

$$\begin{aligned} \text{Disc}[f(x)] &= -4a_1^3 a_3 - 27a_0^2 a_3^2 + a_1^2 a_2^2 \\ &\quad + 18a_0 a_1 a_2 a_3 - 4a_0 a_2^3. \end{aligned} \quad (\text{A5})$$

Appendix B: Relation between symmetry indicators

Parity eigenvalues are implicitly involved with indicators defined in Eqs. (7) and (16). In addition, exceptional points captured by these indicators correspond to

the gapless nodes in Hermitian systems with chiral symmetry.

Firstly, let us consider the following Hamiltonian

$$\tilde{h}(\mathbf{k}) = \begin{pmatrix} 0 & \Delta(\mathbf{k}) \\ \Delta^*(\mathbf{k}) & 0 \end{pmatrix}. \quad (\text{B1})$$

The exceptional point emerge when $\Delta(\mathbf{k}) = 0$ holds which is described by zero modes of Eq. (B1). We note that $\tilde{h}(\mathbf{k})$ satisfies

$$\sigma_1 \tilde{h}(\mathbf{k}) \sigma_1 = \tilde{h}(-\mathbf{k}), \quad (\text{B2a})$$

$$\sigma_3 \tilde{h}(\mathbf{k}) \sigma_3 = -\tilde{h}(\mathbf{k}), \quad (\text{B2b})$$

which means that $\tilde{h}(\mathbf{k})$ preserves inversion and chiral symmetry. Equation (B2a) holds due to Eq. (6).

We note that $\Delta(\mathbf{k})$ is real at TRIM. In addition, Eq. (B2a) indicates that the sign of $\Delta(\mathbf{k})$ corresponds to the parity eigenvalue for the occupied state (i.e., the eigenstate of $\tilde{h}(\mathbf{k})$ whose eigenvalue is negative). In this sense, Eqs. (7) and (16) implicitly compute parity eigenvalues of occupied states.

Correspondence between the exceptional points and gapless excitations for Hermitian systems can be seen in the following relation

$$\zeta_{1,2D} = (-1)^{z_{1,4}}, \quad (\text{B3a})$$

$$\zeta_{1,3D} = (-1)^{z_{1,8}}, \quad (\text{B3b})$$

where indicators z_{14} and z_{18} are defined below. Noting that the indicators $z_{14(8)}$ predicts gapless excitations in the two- (three-) dimensional Hamiltonian (B1)^{58,62}, we can see that exceptional points correspond to these gapless excitations.

Indicators z_{14} and z_{18} are defined as follows. Consider a Hermitian system satisfying

$$U_I \tilde{h}_0(\mathbf{k}) U_I = \tilde{h}_0(-\mathbf{k}), \quad (\text{B4})$$

$$U_C \tilde{h}_0(\mathbf{k}) U_C = -\tilde{h}_0(\mathbf{k}), \quad (\text{B5})$$

with unitary matrices which satisfy $U_I^2 = U_C^2 = \mathbb{1}$ and $U_I U_C = -U_C U_I$. Symmetry indicator of such a system is discussed in Refs. 58 and 62. In two dimensions, the \mathbb{Z}_4 -indicator is defined as

$$z_{14} := \frac{1}{2} \sum_{\mathbf{k} \in \text{TRIM}} (N_{\mathbf{k}}^+ - N_{\mathbf{k}}^-) \pmod{4}, \quad (\text{B6})$$

where $N_{\mathbf{k}}^{+(-)}$ denotes the number of occupied bands with the positive (negative) parity at $\mathbf{k} \in \text{TRIM}$. For $z_{14} = 1, 3$, the system is gapless due to the chiral symmetry^{58,62}. In three dimensions, the \mathbb{Z}_8 -indicator is defined as

$$z_{18} := \frac{1}{2} \sum_{\mathbf{k} \in \text{TRIM}} (N_{\mathbf{k}}^+ - N_{\mathbf{k}}^-) \pmod{8}. \quad (\text{B7})$$

For odd z_{18} , the system shows gapless lines due to the chiral symmetry.

Now, we prove Eq. (B3) by focusing on the two-dimensional case. Firstly, we note that $N_{\mathbf{k}}^+ + N_{\mathbf{k}}^- = N_{\text{occ}}$.

holds where $N_{\text{occ.}}$ denotes the number of occupied states. Thus, we have $z_{\text{I},4} = 2N_{\text{occ.}} - \sum_{\mathbf{\Gamma}_j} N_{\mathbf{\Gamma}_j}^-$, which results in

$$(-1)^{z_{\text{I},4}} = \prod_{\mathbf{\Gamma}_j \in \text{TRIM}} (-1)^{N_{\mathbf{\Gamma}_j}^-}. \quad (\text{B8})$$

Applying the above relation to the Hamiltonian (B1), we have

$$(-1)^{z_{\text{I},4}} = \prod_{\mathbf{\Gamma}_j \in \text{TRIM}} \text{sgn} \Delta(\mathbf{\Gamma}_j), \quad (\text{B9})$$

which is equivalent to Eq. (B3a). In a similar way we can prove Eq. (B3b).

The above results elucidate that exceptional points captured by the discriminant indicators correspond to gapless excitations of $\tilde{h}(\mathbf{k})$ captured by indicators for Hermitian systems.

Appendix C: Eq. (25) \Rightarrow Eq. (23)

Supposing that Eq. (25) holds, we can prove Eq. (23) as follows. Firstly, we note that Eq. (25) connects the

energy eigenvalues at \mathbf{k} and at $-\mathbf{k}$

$$\epsilon_n(-\mathbf{k}) = \epsilon_n^*(\mathbf{k}), \quad (\text{C1a})$$

$$\epsilon_n(\mathbf{k}) = \epsilon_n(-\mathbf{k}). \quad (\text{C1b})$$

As the discriminant is computed from the eigenvalues [see Eq. (3)], we obtain Eq. (23).

In the following, we prove Eq. (C1). The condition of the time-reversal symmetry results in Eq. (C1a), which can be seen as follows. Suppose that $|R_n(\mathbf{k})\rangle$ are right eigenvectors with eigenvalue $\epsilon_n(\mathbf{k})$. Then, we have

$$\begin{aligned} H(-\mathbf{k})U_{\text{T}}\mathcal{K}|R_n(\mathbf{k})\rangle &= U_{\text{T}}H^*(\mathbf{k})\mathcal{K}|R_n(\mathbf{k})\rangle \\ &= U_{\text{T}}\mathcal{K}H(\mathbf{k})|R_n(\mathbf{k})\rangle \\ &= \epsilon_n^*(\mathbf{k})U_{\text{T}}\mathcal{K}|R_n(\mathbf{k})\rangle. \end{aligned} \quad (\text{C2})$$

Here, in the first line we have used Eq. (25a). Thus, we obtain Eq. (C1a).

In a similar way we can prove Eq. (C1b). Because the relation

$$\begin{aligned} H(-\mathbf{k})U_{\text{I}}|R_n(\mathbf{k})\rangle &= U_{\text{I}}H(\mathbf{k})|R_n(\mathbf{k})\rangle \\ &= \epsilon_n(\mathbf{k})U_{\text{I}}|R_n(\mathbf{k})\rangle, \end{aligned} \quad (\text{C3})$$

holds, we obtain Eq. (C1b). Here, in the first line, we have used Eq. (25b).

The above facts prove that Eq. (23) holds when the Hamiltonian satisfies Eq. (25).